Nanoparticle-encapsulated siRNAs for gene silencing in the haematopoietic stem-cell niche

Marvin Krohn-Grimberghe[1,2,&], **Michael J. Mitchell**[3,4,&], **Maximilian J. Schloss**[1,&], **Omar F. Khan**[3], **Gabriel Courties**[1], **Pedro P.G. Guimaraes**[3], **David Rohde**[1], **Sebastian Cremer**[1], **Piotr S. Kowalski**[3], **Yuan Sun**[1], **Mingchee Tan**[3], **Jamie Webster**[3], **Karin Wang**[5], **Yoshiko Iwamoto**[1], **Stephen P. Schmidt**[1], **Gregory R. Wojtkiewicz**[1], **Ribhu Nayar**[1], **Vanessa Frodermann**[1], **Maarten Hulsmans**[1], **Amanda Chung**[5], **Friedrich Felix Hoyer**[1], **Filip K. Swirski**[1], **Robert Langer**[3], **Daniel G. Anderson**[*,3,&], **Matthias Nahrendorf**[*,1,6,7,&]

[1]Center for Systems Biology, Massachusetts General Hospital and Harvard Medical School, Simches Research Building, 185 Cambridge Street, Boston, MA 02114, USA

[2]Department of Cardiology and Angiology I, Heart Center Freiburg University, Freiburg, Germany

[3]Department of Chemical Engineering, David H. Koch Institute for Integrative Cancer Research, MIT, Cambridge, MA 02139, USA

[4]Department of Bioengineering, University of Pennsylvania, Philadelphia, PA 19104, USA

[5]Molecular and Integrative Physiological Sciences, Harvard T.H. Chan School of Public Health, Boston, MA 02115, USA

[6]Cardiovascular Research Center, Massachusetts General Hospital and Harvard Medical School, Boston, MA, USA.

[7]Department of Internal Medicine I, University Hospital Wuerzburg, Wuerzburg, Germany.

Abstract

[*]**Correspondence and requests for materials** should be addressed to Matthias Nahrendorf (mnahrendorf@mgh.harvard.edu) or Daniel Griffith Anderson (dgander@mit.edu).
[&]These authors contributed equally

Bone-marrow endothelial cells in the haematopoietic stem-cell niche form a network of blood vessels that regulates blood-cell traffic as well as the maintenance and function of haematopoietic stem and progenitor cells. Here, we report the design and in vivo performance of systemically injected lipid–polymer nanoparticles encapsulating small interfering RNA (siRNA), for the silencing of genes in bone-marrow endothelial cells. In mice, nanoparticles encapsulating siRNA sequences targeting the proteins stromal derived factor 1 (Sdf1) or monocyte chemotactic protein 1 (Mcp1) enhanced (when silencing Sdf1) or inhibited (when silencing Mcp1) the release of stem and progenitor cells and of leukocytes from the bone marrow. In a mouse model of myocardial infarction, nanoparticle-mediated inhibition of cell release from the haematopoietic niche via Mcp1 silencing reduced leukocytes in the diseased heart, improved healing after infarction, and attenuated heart failure. Nanoparticle-mediated RNA interference in the haematopoietic niche could be used to investigate haematopoietic processes for therapeutic applications in cancer, infection and cardiovascular disease.

Human bone marrow harbors about 10,000 bona fide hematopoietic stem cells as well as millions of downstream progenitors and releases billions of blood cells into the circulation every day[1,2]. The organ produces a cellular ensemble that accomplishes vital tasks including oxygen transport, defense against pathogens and clotting[1,3]. The activities of its inhabitants, such as cell quiescence, proliferation, differentiation and migration, are adjusted to current systemic needs and regulated by non-hematopoietic bone marrow niche cells[3,4]. This cast of supporting cells includes endothelial cells, which instruct hematopoietic cell behavior via a mix of soluble and cell surface-bound signals[1,2,5,6]. Niche cells receive circulating and neuronal signals from outside the marrow and relay them to hematopoietic stem and progenitor cells (HSPC)[7].

Over the past decade, many niche cell steady-state functions have been discovered, leading to approved drugs for stem cell mobilization prior to transplantation[8]. Drugs such as Filgrastim that disrupt the interactions between SDF1 and its receptor CXCR4 on leukocytes and HSPCs are now widely utilized as agents to mobilize stem cells into the bloodstream for bone marrow transplantation[9]. Such agents have primarily been applied in the realm of hematology/oncology; however, recent evidence suggests that leukocyte and HSPC release from bone marrow plays an essential role in many other chronic inflammatory conditions, including cardiovascular disease[10]. Broadly speaking, the number of circulating leukocytes and the production of blood components in the hematopoietic niche correlate closely with mortality[10], and if the bone marrow fails altogether, the organism succumbs within a week or two[11,12]. Therefore, technologies that modulate cell behavior within the hematopoietic niche could improve our fundamental understanding and treatment of a range of disease processes that are governed by bone marrow-derived leukocytes.

RNA interference (RNAi) therapeutics are a potentially attractive means to influence protein expression within the hematopoietic niche, as they can be used to silence nearly any gene within the body to achieve therapeutic effects[13]. Currently, the most advanced RNAi therapeutic is patisiran, a small interfering RNA (siRNA) lipid nanoparticle-based drug[14]. Patisiran, recently approved by the FDA, inhibits hepatic transthyretin production as a form of transthyretin amyloidosis therapy[14]. Because the gene sequences are known, siRNA drugs

can be screened for in silico, produced and validated within very short time spans. However, while potent siRNAs can be rapidly identified, systemic delivery to the appropriate tissue can prove challenging. The use of RNAi to treat disease requires effective methods of targeted delivery, as "naked" siRNAs are unstable in the bloodstream and do not readily traverse cell membranes[13].

With significant advantages over their non-formulated and free drug counterparts, nanoparticle delivery systems have been used effectively as delivery vehicles in several medical settings[15]. For siRNA delivery, nanoparticle's key advantages are: (i) preventing nucleic acid degradation by serum endonucleases in blood, (ii) avoiding renal clearance from the bloodstream, (iii) delivering cargo to specific cells by tailoring nanoparticle surface chemistry and (iv) mediating target cell entry and endosomal escape to enable nucleic acid release into the cytoplasm[13,16]. Delivery materials differ in efficiency, toxicity and biodistribution, and certain nanoparticles have avidity to certain cell types, tissues and organs[17], particularly to hepatocytes, leukocytes and endothelial cells[18–24]. Of note, our group previously reported a nanoparticulate formulation consisting of low molecular weight polyamines and lipids that mediated potent gene silencing in endothelial cells residing in the lung[19].

Here we describe the development of an siRNA formulation capable of delivering siRNA to endothelial cells in the hematopoietic niche. We first screened a library of nanoparticles based on a class of nanoparticle-forming materials that were generated by combinatorial chemical synthesis and deliver siRNA to lung endothelium in vivo[19,25]. These materials were synthesized by reacting low-molecular weight polyamines with epoxide-terminated lipids using an epoxide ring-opening reaction[19]. By screening a library of these nanoparticles in vivo, we developed a polymer-lipid hybrid nanoparticle for delivery to bone marrow endothelial cells. In a series of proof-of-concept experiments, we silence endothelial cell expression of two quintessential hematopoietic niche factors, thereby altering HSPC behavior and systemic leukocyte supply. Such an RNAi approach is of interest to modulating hematopoietic cell activity and abundance in fundamental science and to developing new therapeutics.

Results

Nanoparticle screen for in vivo siRNA delivery to the hematopoietic niche

Bone marrow endothelial cells (BMEC) are an integral component of the hematopoietic niche and instruct stem cell and leukocyte behavior. Cell-specific deletion experiments revealed that both progenitor proliferation and migration are governed by BMEC-derived signals[1,2]. Based on previously reported endothelial cell-avid delivery materials[19], we began developing suitable delivery materials for BMEC. We synthesized a polymer-lipid hybrid material by reacting C15 epoxide-terminated lipids with low molecular weight polyamines (PEI600) at a 14:1 molar ratio via Michael addition chemistry (Fig. 1a). The resulting material was combined with small interfering RNA (siRNA) and a polyethylene glycol (PEG)-lipid conjugate in a high-throughput microfluidic mixing chamber[26] to formulate nanoparticles via electrostatic interactions between the cationic polymeric material and the negatively charged nucleic acid (Fig. 1b). Using this nanomaterial as a starting point, we

then tested different PEG surface coatings that alter biodistribution and pharmacokinetics of various nanoparticle types[27,28]. We hypothesized that modulating nanoparticle PEG architecture enhances nanoparticle siRNA delivery to the bone marrow. By altering their PEG decoration, we created a library of 15 nanoparticle formulations, with three key parameters of the PEG-lipid conjugate modified in each candidate nanoparticle: i) molecular weight of the PEG surface coating (molecular weight range: 2000–5000), ii) PEG surface density, which was altered through varying the overall molar percentage of PEG within the formulation (molar percentage range: 2%–20%) and iii) the length of the lipid chain that anchors PEG within the nanoparticle membrane (Fig. 1c). We injected this mini-library intravenously into mice (1.0 mg/kg body weight) and then assessed Tie2 silencing in the bone marrow. Tie2 as a silencing target was chosen purely for this delivery and silencing assay, and not for the gene's function, which has roles beyond BMEC. Using a branched DNA assay, we identified the best nanoparticle formulation (termed NicheEC-15), which induced ~80% Tie2 in vivo gene silencing in bone marrow (Fig. 1d) without disrupting vascular anatomy (Supplementary Fig. 1). Cryo-scanning electron microscopy and dynamic light scattering showed that NicheEC-15 formed multilamellar nanoparticles (Fig. 1e) with a 60–80 nm diameter (Fig. 1f). We next assessed NicheEC-15 for Tie2 silencing in endothelial cells in vitro. Nanoparticles containing 60 nM Tie2 siRNA induced potent gene silencing in the mouse endothelial cell line bEnd.3 (Fig. 1g) and in primary murine BMEC (Fig. 1h). Confocal microscopic imaging confirmed efficient in vitro uptake of nanoparticles containing fluorescent siRNA (Fig. 1i).

In vivo behavior of the lead particle NicheEC-15

The in vivo blood half life of NicheEC-15, containing a fluorescent siRNA, was measured to be 13.8 minutes by fitting the decrease in blood fluorescence intensity over time after a single i.v. injection (Fig. 2a). Using a range of 0.01 to 1.0 mg/kg siTie2, we observed dose-dependent knockdown of Tie2 mRNA expression by qPCR (Fig. 2b). At a dose of 1 mg/kg siTie2, the knock down achieved with NicheEC-15 was about 50% stronger than 7C1 nanoparticles[19], a previously described nanoparticle with excellent silencing in endothelial cells. A single injection of NicheEC-15 containing 1.0 mg/kg siTie2 induced long-lasting knock down for more than two weeks (Fig. 2c). To better understand the uptake patterns of NicheEC-15, we next directly visualized the hematopoietic niche using intravital microscopy of the skull bone marrow of mice. The vasculature was stained by intravenously injecting a cocktail of PE labeled CD31 and Sca1 antibodies, while Osteosense, a molecular imaging probe that enriches in osteoblasts, outlined the bone surface surrounding hematopoietic niches[29]. Two hours after injecting NicheEC-15-containing fluorescently tagged siRNA, we primarily found the siRNA associated imaging signal in the bone marrow vasculature (Fig. 2d). Cellular distribution of NicheEC-15 was measured by flow cytometric analysis of the bone marrow. While we observed the highest fluorescence intensity in CD45$^-$ CD31$^+$ Sca-1$^+$ endothelial cells, nanoparticle uptake into CD45$^+$ leukocytes was minimal (Fig. 2e). Uptake into other bone marrow cells (Supplementary Fig. 2), and into leukocytes and endothelial cells in other organs (Supplementary Fig. 3a,b) was lower than for BMEC. Such uptake, especially in organs that eliminate drugs or nanoparticles from the blood stream, is to be expected. Macroscopic fluorescence imaging of key organs 2 hours after intravenous injection of NicheEC-15 encapsulating fluorescently labeled siRNA revealed strong

fluorescence in the femur marrow (Supplementary Fig. 3c–f). Compared to a previously described lipidoid nanoparticle with dominant uptake in liver[21] and immune cells[18], NicheEC-15 bone marrow uptake was higher (Supplementary Fig. 3g). The avidity of NicheEC-15 for podoplanin[−] arteriolar and podoplanin[+] sinusoidal BMEC[30] was confirmed by ImageStream (Fig. 2f–i), which indicates uptake into major bone marrow endothelial cell subsets. Cell imaging detected no NicheEC-15 associated fluorescence in bone marrow leukocytes (Fig. 2j–l).

We next benchmarked NicheEC-15 to 7C1[19] in vivo. Compared to 7C1, NicheEC-15 uptake into BMEC increased significantly while uptake into lung endothelial cells decreased (Fig. 2m). While 7C1 uptake was similar in both organs, NicheEC-15 exhibited a three-fold higher uptake into bone marrow endothelial cells (Fig. 2n), a result that supports NicheEC-15's higher avidity for the marrow over the lung. Furthermore, direct comparing Tie2 in lung and bone marrow showed that NicheEC-15 enhanced gene silencing in bone marrow while reducing such effects in lung, compared to 7C1 (Fig. 2o). Such a predilection may allow for high silencing efficiency in the marrow at lower doses.

Sdf1/Mcp1 target screening

Having identified NicheEC-15 as a delivery material, we proceeded to implement RNAi for modulating the hematopoietic bone marrow niche. We began by selecting two target proteins that influence hematopoietic stem cell and leukocyte behavior, specifically stromal derived factor 1 (Sdf1, also known as Cxcl12) and monocyte chemotactic protein 1 (Mcp1, also known as Ccl2). These well-studied proteins[1,2,31,32] were chosen because their known functional properties allowed us to use specific functional in vivo assays; additionally, because these proteins control cellular quiescence and migration, they are interesting drug targets. Viable siRNA sequences targeting Sdf1 (Supplementary Fig. 4) and Mcp1 (Supplementary Fig. 5) were identified by in vitro screening of in silico–-predicted candidates. The top four siRNA sequences silencing Sdf1 (Supplementary Fig. 4a, b) and Mcp1 (Supplementary Fig. 5a, b) were then screened in vitro with a dose response assay. The siRNAs with the lowest IC50 and IC80 were selected for scale-up, nanoparticle formulation and modification to minimize immunostimulation and off-target gene silencing[33]. The lead siRNA candidates encapsulated in NicheEC-15 nanoparticles induced potent, dose-dependent gene silencing of Sdf1 (Supplementary Fig. 4c) and Mcp1 (Supplementary Fig. 5c) at low dosages in endothelial cells in vitro.

siSdf1 triggers bone marrow cell release

After tail vein injection of NicheEC-15 loaded with siRNA cargo targeting *Sdf1* (siSdf1), we found a >2-fold decrease in Sdf1 expression (Fig. 3a) and significantly decreased Sdf1 protein in the femur (Supplementary Fig. 6a). To explore the cellular target responsible for this effect, we FACS-isolated bone marrow endothelial cells from mice after treatment with NicheEC-15 containing siSdf1. Indeed, compared to controls, Sdf1 expression was strongly reduced in these cells (Fig. 3b) but not in other niche cells (Supplementary Fig. 6b–d). To evaluate the specificity of RNAi effects, we also examined expression of two other genes that influence HSC behavior in the hematopoietic niche, specifically *Vcam1* and *Scf*. As

expected, no change in gene expression was observed in BMEC, osteoblasts or mesenchymal stromal cells after treatment with siSdf1 (Supplementary Fig. 6e, f).

Since Sdf1 retains HSPC[31] and leukocytes[32] in the bone marrow, we proceeded to investigate HSPC migration to monitor functional consequences of RNAi. Indeed, we observed higher lineage$^-$ sca1$^+$ ckit$^+$ (LSK) cell numbers in blood of mice treated with siSdf1 (Fig. 3c), indicating release of these progenitor cells from the marrow. The increase in circulating HSPC was confirmed by colony forming unit (CFU) assays in blood (Fig. 3d). Accordingly, siSdf1 injection decreased bone marrow LSK cells (Supplementary Fig. 6g, h). Likewise, downstream myeloid progenitors, including common myeloid progenitors (CMP) and granulocyte macrophage progenitors (GMP), declined in numbers in the femur after siSdf1 treatment (Supplementary Fig. 6i–k).

To investigate if RNAi leads to liberation of functional hematopoietic stem cells into the blood, we co-transplanted blood from siSDF1 and PBS treated control mice into lethally irradiated recipients (Supplementary Fig. 7a). Eight weeks later, almost all leukocytes in the blood transplant recipients originated from siSdf1 treated mice (Supplementary Fig. 7b, c). The marrow of primary recipients was then used for a secondary transplantation into lethally irradiated recipient mice. Nine out of ten recipient mice survived for 6 months, after which they exhibited high blood chimerism for major leukocyte subsets (Supplementary Fig. 7d, e). In a head-to-head comparison of RNAi triggered bone marrow stem cell release to the clinical drug AMD3100, which inhibits CXCR4, the cognate receptor of Sdf1, and the growth factor G-CSF, we found siSdf1 treatment effects positioned in between AMD3100 and G-CSF (Supplementary Figure 7f).

In addition to HSPC release, we further detected that siSdf1 treatment leads to monocyte and neutrophil departure from the bone marrow (Fig. 3k–m). As a consequence, neutrophils and monocytes may become more numerous in circulation. Since the level of circulating myeloid cells regulates their presence at sites of inflammation and associates with patient mortality, we studied the early dynamics of this leukocyte release. Two hours after siSdf1 injection, myeloid cells became significantly more abundant compared to baseline, and increased even further at six hours (Fig. 4 a, b). Such a boost in circulating leukocytes may also be caused by redistribution from other cell pools, e.g. in the lung or spleen. Thus we used serial pre- and post-RNAi treatment intravital microscopy to survey the skull bone marrow. We visualized bone marrow macrophages and monocytes in Cx3cr1$^{GFP/+}$ mice before and up to 2.5 hours after siSdf1 injection. By monitoring specific bone marrow niches, we were able to track individual cell behavior over time (Fig. 4c). Treatment with siSdf1 triggered departure of Cx3cr1$^+$ cells, while this was not observed after treatment with control siRNA (Fig. 4d). A similar dynamic was observed for neutrophils that we labeled in vivo with an Ly6g-APC antibody (Fig. 4e, f). In sum, these data demonstrate the ability to trigger stem cell and leukocyte release by silencing retention factors in the bone marrow vasculature.

siMcp1 inhibits bone marrow cell release

While *Sdf1* silencing increased cell migration from the marrow, we next chose a gene target to explore the opposite functionality, i.e. to use RNAi to dampen leukocyte traffic. Such an intervention could be a therapeutic avenue to reducing systemic leukocyte supply in the

setting of inflammation. Monocyte bone marrow departure is triggered by secretion of the chemokine Mcp1 into the sinusoidal space, for instance after infection, injection of lipopolysaccharide, a building block of the bacterial wall that binds toll like receptors, or myocardial infarction[18,34]. Because monocytes express the cognate chemokine receptor Ccr2, they follow the Mcp1 chemokine gradient and extravasate from the niche into the bone marrow sinusoids. We tested the effect of *Mcp1* silencing in the setting of inflammation induced via the injection of lipopolysaccharide (LPS) (Fig. 5a). As expected, LPS injection increased Mcp1 expression in the marrow, and such expression was significantly reduced by siMcp1 treatment (Fig. 5b). Mcp1 protein levels were similarly elevated by LPS, which was abrogated by siMcp1 treatment (Fig. 5c). As a consequence, monocyte numbers in the bone marrow were higher in siMcp1-treated mice (Fig. 5d–f), whereas blood monocyte numbers decreased (Fig. 5g–i).

Mcp1/Ccr2 signaling also regulates monocyte migration in sterile inflammation, including during cardiovascular disease. In particular, acute myocardial infarction triggers blood monocytosis, followed by cell recruitment into the ischemic myocardium[35]. After MI, systemic oversupply of inflammatory monocytes may lead to heart failure and subsequent ischemic events[10]. We therefore tested if silencing Mcp1 in mice with acute MI may reduce inflammatory Ly6c^{high} monocyte numbers in circulation and the heart. Treating mice with siMcp1 led to a lower bone marrow Mcp1 expression (Fig. 6a) and protein level (Fig. 6b). Consequently, monocyte bone marrow numbers rose (Fig. 6c, d) while circulating monocyte numbers remained lower (Fig. 6f–h), results that indicated attenuated cell release from the marrow. Ultimately, fewer monocytes, including the inflammatory Ly6C^{high} subset, were recruited to the infarcted heart in mice treated with siMcp1 (Fig. 6i–k).

We evaluated the therapeutic consequences of siMcp1 on cardiovascular outcomes by studying the recovery from myocardial infarction in ApoE$^{-/-}$ mice with hypercholesterolemia and atherosclerosis. In these mice, gene deletion and high fat diet leads to blood monocytosis that arises from increased hematopoiesis[36–38]. We previously described that the oversupply of monocytes in the post-MI phase disrupts resolution of inflammation after cardiac ischemia, leading to poor infarct healing and increased severity of heart failure[39,40]. Thus, these mice, like patients with atherosclerosis, hyperlipidemia and monocytosis, hypothetically benefit from a dampened leukocyte supply to the infarct. ApoE$^{-/-}$ mice were given an atherogenic diet for 10 weeks prior to permanent coronary ligation. Mice were treated either with 3 doses control siRNA or siMcp1. We examined infarct healing histologically 7 days after coronary ligation. In line with the flow cytometry data described above, RNAi treatment reduced staining for CD11b$^+$ myeloid cells in the border zone and the infarct core (Fig. 7a–d). We further observed a reduction of fibroblast numbers and collagen content in the border zone, indicating that the treatment reduced inflammation and fibrosis.

Additional cohorts of ApoE$^{-/-}$ mice were examined 3 weeks after MI, when left ventricular remodeling gives rise to heart failure. Cardiac MRI reported that siMcp1 treatment preserved left ventricular anatomy and function when compared to siLuc treated control ApoE$^{-/-}$ mice (Fig. 8a–e). Masson's trichrome staining revealed that the percentage of the left ventricle occupied by scar was lower in siMcp1 treated mice (Fig. 8f, g). Taken together, these data

implicate that reduction of systemic monocyte supply by RNAi augmented recovery from myocardial infarction.

Discussion

Bone marrow niche cells regulate hematopoietic and leukocyte activity in numerous ways, including cell transit into the circulation[1,2,41]. We have developed a nanoformulation capable of delivering siRNA to bone marrow niche cells. These nanoparticles are derivatives of prior materials with avidity for lung endothelial cells[19]. We enhanced nanoparticle siRNA delivery to the bone marrow by modulating nanoparticle PEG architecture, including i) the molecular weight of the PEG surface coating, ii) the length of the lipid chain that anchors PEG within the nanoparticle membrane and iii) PEG surface density. By screening polymer-lipid hybrid materials, combined with modulating PEG nanoparticle surface coatings, we obtained a nanoparticle, termed NicheEC-15, with superior avidity for and efficient silencing in bone marrow endothelial cells. We speculate that NicheEC-15, perhaps due to its denser PEG surface coat, escapes first pass entrapment in the lung, which increases arterial circulation and uptake into bone marrow endothelial cells. The mechanism of uptake into bone marrow endothelial cells remains to be determined and may be subject to changes induced by pathologies or treatments such as irradiation or chemotherapy.

To test NicheEC-15, we silenced two prototypical hematopoietic niche factors. One of them, Sdf1, promotes stem cell quiescence and bone marrow retention of leukocytes via interaction with its cognate receptor Cxcr4. This pathway is currently targeted clinically using G-CSF and AMD3100, which trigger stem cell liberation into the blood[42]. Silencing HSPC retention factors using nanoparticle enabled RNAi may improve the cell yield in stem cell transplantation, especially in patients that are poor stem cell mobilizers due to comorbidities such as diabetes[43]. Our second target, Mcp1, has the opposite effect, as this chemokine triggers bone marrow monocyte release. We found that silencing those proteins, using NicheEC-15 enabled RNAi, altered migration of HSPC and leukocytes from bone marrow niches into the systemic blood pool. Our data provide proof-of-principle that bone marrow HSPC and leukocyte behavior may be addressed using RNAi therapeutics with avidity for the hematopoietic niche.

Due RNAi's modular character, this approach can be adapted for silencing any other endothelial cell derived bone marrow niche factor, including growth hormones, cytokines and adhesion molecules that influence HSPC or leukocyte biology. Furthermore, silencing receptors may modulate endothelial cells' ability to sense and relay information they receive from the circulation. The function of bone marrow niche cells in steady state and disease is the subject of vibrant research, and large unbiased data-sets, for instance obtained by RNA sequencing of bone marrow endothelial cells, are increasingly becoming available[44]. The technology we describe here is suitable for rapidly testing the function of highly expressed genes and newly arising drug candidates in vivo.

Endothelial cells separate bone marrow niches from the blood pool. Their barrier function, which ultimately regulates cell release, make them a particularly attractive target for modulating cell migration. However, there are other niche cells that regulate hematopoiesis.

Future materials may deliver siRNA to bone marrow macrophages, mesenchymal stromal cells or osteoblasts, thereby targeting other niche components. Such additions to the target cell portfolio may also facilitate RNAi for niche-driven malignancies.

While we focused on bone marrow cell release, which is of clinical interest in harvesting stem cells prior to autologous hematopoietic bone marrow transplantation for leukemia treatment, other hematopoietic cell functions could also be influenced. Stem cell quiescence and lineage bias are of particular interest as they decisively influence the size and function of any systemic blood cell pool. As demonstrated by silencing *Mcp1*, reducing the release of short-lived leukocytes from their site of production may dampen inflammation at any inflammatory site, including the ischemic heart. Thus, reducing the oversupply of innate immune cells may curtail exuberant inflammatory activity in cardiovascular disease[10], the leading cause of death worldwide.

Methods

Polymer-lipid hybrid synthesis

Polymer-lipid hybrids were synthesized by reacting C15 alkyl epoxides (Tokyo Chemical Industry and Sigma) with PEI600 at 90 °C in 100% ethanol for 48–72 hours at a 14:1 molar ratio. Due to the polydispersity of PEI600 (Mn=600, PDI = 0.33), polymer-lipids were purified via high performance liquid chromatography (HPLC) on a silica column with DCM. MeOH and NH4OH were added to the solvent over a 45 minute period to decrease polarity, which enabled HPLC separation of the polymer-lipid into fractions related to the hydrophobic C15: hydrophilic PEI ratio. Mixtures were split into five fractions and individually assessed for their ability to induce gene silencing in mice.

siRNA nanoparticle synthesis

To formulate nanoparticles, polymer-lipid materials were combined with polyethylene (PEG)-lipid conjugates (Avanti Polar Lipids) and mixed with siRNA in a microfluidic device. Polymer-lipids and PEG-lipid conjugates were dissolved in 200 proof ethanol and loaded into a gas-tight Hamilton glass syringe, while siRNA were in an 10 mM citrate buffer (pH 3.0; Teknova). Syringes were connected to inlets of a microfluidic device containing static mixers, and contents were perfused through the device to formulate nanoparticles. Nanoparticle formulations were sterile filtered against PBS using a MW 20,000 cutoff dialysis cassette (Thermo Scientific) to remove citrate and ethanol. Nanoparticle size and structure were determined by both dynamic light scattering (DLS) using a Zetasizer Nano ZS machine (Malvern Instruments) and cryo-transmission electron microscopy (TEM) using a Tecnai 12 G2 TEM (FEI). Nanoparticle samples were prepared in a vitrification system (25°C, ~100% humidity), and images of samples were recorded on an UltraScan 1000 CCD camera (Gatan) in low dose conditions. For zeta potential measurements, nanoparticles (25 µL) at a polymer-lipid concentration of 1 mg/mL were added to PBS (1 mL) and measured using a Malvern Zetasizer Nano ZS machine (mean, –0.15 mV; std, 9.28). The concentration of siRNA used for in vitro and in vivo treatment was quantified using both a Quant-iTTM Ribogreen assay (Invitrogen) and NanoDrop measurement (Thermo Scientific).

Cell culture

The endothelial cell line bEnd.3 (CRL-2299, ATCC) was cultured in Dulbecco's modified Eagle's medium, supplemented with 10% (vol/vol) fetal bovine serum and 1% (vol/vol) penicillin/streptomycin under humidified conditions at 37°C and 5% CO_2 until cell confluence. To investigate knock down efficiency, bEnd.3 cells were plated in 24 well plates (150,000 cells per well) and incubated for 24 hours prior to treatment with nanoparticles formulated with siRNA targeting one of the following genes: luciferase (LUC), monocyte chemoattractant protein-1 (Mcp1) or stromal-derived factor-1 (Sdf1). A serial dilution of each siRNA nanoparticle formulation in PBS was prepared at concentrations of 1–60 nM of siRNA. Samples were then incubated for 24 hours prior to gene expression analysis. Cells were washed with PBS and harvested using 0.25% trypsin. RNA was extracted from cells using a Arcturus PicoPure RNA Isolation Kit (Thermo Scientific). To study the in vitro uptake of NicheEC-15 by microscopy, bEnd.3 cells were plated in 6 well plates (500,000 cells per well) and grown until confluence. NicheEC-15 containing Alexa Fluor 647 coupled luciferase siRNA was then added at a concentration of 200 nM RNA 2 hours before imaging. 15 minutes before imaging 5 μM Syto 13 Green (Life Technologies) and 5 μg/ml wheat germ agglutinin Alexa Fluor 555 (WGA, Life Technologies) were added. During the last 5 minutes the cell cultures were washed repeatedly with PBS. The controls were treated identically, except that NicheEC-15 containing unlabelled luciferase siRNA was used. All steps except washing were done under humidified conditions at 37°C and 5% CO_2.

Mice

All animal procedures conducted at MGH and MIT were approved by the Institutional Animal Care and Use Committees (IACUC) and were in accordance with local, state and federal regulations. C57BL/6J(Jackson Laboratory, stock # 000664), B6.129P-Cx3cr1[tm1Litt/J] (Jackson Laboratory, stock # 005582), B6.SJL-Ptprc[a]Pepc[b]/BoyJ (Jackson Laboratory, stock # 002014) mice were used at 11 to 13 weeks of age. To receive hemizygous B6.129P-Cx3cr1[tm1Litt/J] mice, homozygous mice were crossed with C57BL/6J mice. Nanoparticles were administered by tail vein injection. Myocardial infarction was induced by permanent coronary ligation in B6.129P2-Apoe[tm1Unc]/J (Jackson Laboratory, stock # 002052) after 10 weeks of high fat diet (Envigo Teklad Diets, stock #TD.88137), starting at 8 weeks of age and done as previously described[29]. Briefly, mice were anaesthetised, given buprenorphin subcutaneously for analgesia, intubated and ventilated with 2% isoflurane supplemented with oxygen. After thoracotomy, the heart was exposed, and the left coronary artery was identified, and permanently ligated with a monofilament nylon 8–0 suture. For the LPS model, after nanoparticle treatment, 100 μl normal saline containing 2 ng LPS (Sigma) was injected i.v. and the mice harvested 4 hours after LPS injection.

Gene silencing

For gene silencing in whole femoral bone marrow, mice were sacrificed by CO_2 asphyxiation, and femurs were harvested and immediately snap-frozen in liquid nitrogen. Frozen tissues were pulverized to form a powder using a SPEX 2010 Geno/Grinder (SPEX SamplePrep). Tissue lysates were prepared in Tissue and Cell Lysis Buffer (Epicentre)

supplemented with 0.5 mg/mL Proteinase K (Epicentre). Tissue samples were mixed at 1400 RPM for 2 h at 65°C and centrifuged at 16,000 RCF to remove bone debris. mRNA levels in the supernatant were quantified using the QuantiGene 2.0 luminescent-based branched DNA (bDNA) assay kit and the QuantiGene 2.0 probes against Tie2 and GAPDH (Thermo Fisher Scientific) according to the manufacturer's protocol. Luminescent signals were measured using a Tecan Infinite 200 PRO plate reader (Tecan). Standard curves for femur tissues and each target gene were constructed using samples from untreated mice to ensure optimal dilutions for assay samples that avoid luminescent signal saturation. Targeted gene silencing in treated mice was quantified by calculating the ratio of target gene luminescence to Gapdh gene luminescence, with all values normalized to target gene:Gapdh gene ratios from control mice.

Flow cytometry and sorting

Single-cell suspensions were obtained from peripheral blood, bone marrow, aorta and lung. Briefly, blood was collected by eye bleeding using heparinised capillaries or, if larger volumes were needed, by cardiac puncture and addition of 10 mmol/L EDTA per 100 µl of blood. Red blood cells lysis was achieved by adding 1x red blood cell lysis buffer (Biolegend) for 2 minutes. After blood collection, mice were perfused through the left ventricle with 30 mL ice-cold PBS after cutting the inferior vena cava. Bone marrow was harvested by flushing femurs in PBS with 0.5% bovine serum albumin (BSA) for leukocyte and HSPC staining or with HBSS containing 2 mg/ml Dispase (Sigma), DNaseI (Sigma) and 1 mg/ml collagenase IV and incubated with gentle agitation for 30 minutes at 37°C to extract endothelial cells. To extract endothelial cells from solid tissues, organs were minced with a fine scissor and incubated in the same digestion mix as bone marrow. Osteoblasts were harvested by crushing the femur and digesting the bone fragments in PBS with 1 mg/ml collagenase I (Gibco) and DNaseI (Sigma) Tissues were then plunged thorough 70-µm nylon mesh (BD Falcon), washed and centrifuged (8 minutes; 300g; 4°C). The obtained single cell suspensions were stained at 4°C for 30 minutes and afterwards washed, centrifuged and resuspended. Fluorochrome- and biotin-conjugated antibodies specific to mouse B220 (clone RA3–6B2), CD3e (clone 145–2C11), CD4 (clone GK1.5), CD8a (clone 53–6.7), CD11b (clone M1/70), CD11c (clone HL3), CD16/32 (clone 93 and 2.4G2), CD19 (clone 1D3), CD31 (clone MEC13.3), CD34 (clone RAM34), CD41 (clone MWReg30), CD45 (clone 30-F11), CD45.1 (clone A20), CD45.2 (clone 104), CD51 (BioLegend, #104106, clone RMV-7), CD48 (HM48–1), CD90.2 (clone 53–2.1), CD115 (clone AFS98), CD150 (clone TC15–12F12.2), c-kit (clone 2B8), F4/80 (clone BM8), GR1 (clone RB6–8C5), IL7Rα (clone A7R34), Ly6C (clone AL-21), Ly-6G (clone 1A8), NK1.1 (clone PK136), PDGFRa (CD140a, clone APA5), podoplanin (clone 8.1.1), Sca-1 (clone D7) and Ter-119 (clone TER-119) were used. Antibodies were purchased from Biolegend, BD Biosciences or eBioscience. Monocytes were identified as $CD90^-$ $CD19^-$ $NK1.1^-$ $Ly-6G^-$ $D45.2^+$ $CD11b^{high}$ $CD115^+$ $F4/80^{low}$ and separated into $Ly-6C^{low}$ and a $Ly-6C^{high}$ populations. Neutrophils were identified as $CD90^-$ $CD19^-$ $NK1.1^-$ $D45.2^+$ $CD11b^{high}$ $Ly-6G^+$, T cells as $CD11b^-$ $CD19^-$ $NK1.1^-$ $CD45^+$ $CD90/CD4^+$ and B cells as $CD11b^-$ $CD90/CD4^-$ $NK1.1^-$ $CD45^+$ $CD19^+$. Blood and bone marrow LSK were identified as (B220 CD3e CD4 CD8a CD11b CD11c CD19 CD90.2 GR1 IL7Ra NK1.1 Ter119)$^-$ $c-kit^+$ $Sca-1^+$, LKs as (B220 CD3e CD4 CD8a CD11b CD11c CD19 CD90.2 GR1 NK1.1 Ter119)$^-$ $c-kit^+$

Sca-1$^-$ and subdivided into CMP, MEP and GMP by their CD16/32 and CD34 expression. Endothelial cells were gated as CD45.2$^-$ Ter119$^-$ CD31$^+$ Sca-1$^+$. Sinusoidal endothelial cells where distinguish by podoplanin expression (podoplanin$^+$) from arteriolar endothelial cells (podoplanin$^-$). Osteoblasts were gated as CD45$^-$ Ter119$^-$ CD31$^-$ PDGFRa$^+$ CD51$^+$ Sca1$^-$ and mesenchymal stromal cells (MSC) as CD45$^-$ Ter119$^-$ CD31$^-$ Sca1$^-$ Lepr^{YFP+}. To define positivity for AF647-siRNA uptake we used cells from uninjected mice as a negative control. Data were acquired on an LSRII (BD Biosciences) and analysed with FlowJo software (Tree Star). For cell sorting the populations were defined as described and sorted using a FACSAria II cell sorter. The cells were directly sorted into lysis buffer, and the samples were vortexed, quick frozen on dry ice and stored at −80°C until RNA extraction.

mRNA Extraction and qPCR

Messenger RNA (mRNA) extraction and qPCR was performed as published before and is reproduced from ref[29]. mRNA was extracted from cells using a Arcturus PicoPure RNA Isolation Kit (Thermo Scientific) for cultured and sorted endothelial cells, and the RNeasy Mini Kit (Qiagen) was used for whole bone marrow samples, both according to the manufacturers' protocols. mRNA concentration was measured using a NanoDrop 2000c Spectrophotometer (Thermo Scientific) or using a 2100 Bioanalyzer (Agilent) for low mRNA concentration. Yield was calculated and the same amount of mRNA was transcribed to complementary DNA (cDNA) using the high capacity RNA to cDNA kit and Taqman primers (all Applied Biosystems). Results were expressed as Ct values after normalization to Gapdh as the housekeeping gene.

Imaging flow cytometry (IFC) data acquisition and analysis

We used an ImageStream^x MkII Imaging flow cytometer (IFC) (Amnis Corporation, Seattle, WA, USA) equipped with two cameras and twelve channels to acquire images from bright-field (BF/Ch-01 or Ch-09) and dark-field (SSC/Ch-12) channels for each cell. INSPIRE version 200.1.620.0 instrument software was used for instrument setup, calibration and data acquisition. Laser power settings were as follows: 405nm at 80mW; 488nm at 150mW; 642nm at 150mW 785nm (SSC) at 1.00mW, 100–150uL samples were loaded and multiple 100,000 event files were acquired at 60x magnification for each sample. The acquired RIF files were later merged and analyzed using IDEAS® version 6.2.64.0 software. 1,000 event single color compensation controls were collected (w/o BF or SSC) and later merged to create a compensation matrix for analysis. Once the RIF files were merged and compensated, a gating strategy similar to the flow cytometry gating of BMEC was used for consistency: a bivariate plot of CD45/Ter119 vs SSC was first generated. Events negative for CD45/Ter119 were then used as a parent population for the generation of a bivariate plot of Sca-1 vs CD31. Double positive events were gated, visually verified as ECs and confirmed to contain NanoParticle AF647 by imagery.

Drug induced stem cell release assay

To compare the release of stem cells into the peripheral blood after siSDF1, AMD3100 and GCSF treatment four groups of mice were formed. The control group received no injections, the siSDF1 group was treated once daily with 2 mg/kg siSDF1 for 3 consecutive days and

harvested 24 hours after the last injection. In the AMD3100 group mice received an injection of 5 mg/kg 3 hours before harvest and in the GCSF group mice were treated for 5 consecutive days with 250 μg/kg daily and harvested 12 hours after the last injection. All mice were harvested at the same time and 100 μl of peripheral blood was drawn for CFU assay.

Colony-forming unit assay

Colony-forming unit (CFU) assays were performed using a semisolid cell culture medium (Methocult M3434, Stem Cell Technology) following the manufacturer's protocol. 100 μl whole blood were processed following the protocol, plated on 35-mm plates in duplicates and incubated for 10 days. Colonies were counted using a low-magnification inverted microscope.

Competitive peripheral blood transplantation and secondary bone marrow transplantation

For the primary, competitive peripheral blood transplantation[45–47] CD45.1+ mice received lethal irradiation (9.5 Gy) 24 hour before transplantation. CD45.2+ donor mice received consecutive injections of 2 mg/kg siSDF1 every 24 hours for three days while another batch of CD45.1+ control mice were injected with PBS. 24 hours after the last injection, the blood of the siSDF1 treated CD45.2+ and the CD45.1+ control mice was collected by cardiac puncture, red blood cells were lysed by adding red blood cell lysis (RBCL) buffer for 2 minutes, the cells were washed by adding 20 ml of cold PBS, spun down (5 min, 300 rpm) and resuspended for counting. 1×10^8 nucleated blood cells from CD45.2+ and CD45.1+ mice were pooled and injected through the tail vein into the lethal irradiated recipient mice. 8 weeks later, the blood chimerism was analyzed by drawing 50μl of blood for flow cytometry.

For the secondary transplant, another batch of CD45.1+ recipient mice were lethally irradiated (9.5 Gy) 24 hours before the transplantation. On the day of the transplantation, femoral bones of the mice from the first, competitive blood transplantation experiment were harvested. The bone marrow was flushed out with cold PBS, plunged through a 40μm cell strainer and centrifuged (5 min, 300 rpm), red blood cells were lysed for 2 minutes with RBCL buffer, centrifuged again and resuspended in PBS with 5% albumin for counting. Each lethally irradiated, secondary recipient CD45.1+ recipient mouse was transplanted with 5×10^6 bone marrow cells by tail vein injection. Six months after secondary transplantation blood chimerism was analyzed by drawing 50μl of peripheral blood.

Fluorescence Reflectance Imaging (FRI)

For biodistribution imaging, mice were sacrificed 2 hours after injection of 2mg/kg encapsulated siRNA labeled with a near infrared fluorochrome. Main organs were then harvested and imaged on a planar fluorescent reflectance imaging system (OV-110, Olympus) with an excitation wavelength of 630nm and exposure times of 60–75 msec.

Intravital microscopy

To visualize in vivo uptake of NicheEC-15 in bone marrow endothelial cells we imaged the skull bone marrow as described before[29]. Osteosense was injected i.v. 24 hours, NicheEC-15 AF647-siRNA 2 hours and PE labeled CD31 and Sca1 antibodies 1 hour before imaging.

MRI

ApoE$^{-/-}$ mice were kept on high fat diet for 10 weeks starting at an age of 8 weeks before induction of MI by permanent ligation of the left coronary artery. Mice were treated with either siMCP1 or control siLUC (2 mg/kg) 4 days before MI, the day of MI induction and 2 days after induction. Mice were imaged 21 days after infarct induction on a Bruker 4.7 Tesla Pharmascan magnetic resonance imaging system with a stack of contiguous short axis slices covering the entire left ventricle. We used a cine intragate fast low angle shot (FLASH) sequence with the following parameters: echo time: 2.945 ms, repetition time: 12.0 ms, flip angle: 45 deg, oversampling 300, matrix size 200×200, pixel size: 0.150×0.150 mm, slice thickness: 1 mm, number of movie frames per cycle: 16. The left ventricular myocardium and cavity were segmented manually at diastole and systole using Horos software to calculate the ejection fraction and volume of the left ventricle. In addition, the percentage of the left ventricle that was infarcted was also determined manually by segmenting the infarct area.

Histology

To investigate bone marrow vessel density, mice were euthanized and femurs were removed 7 days after injection of siSDF1 (2 mg/kg), siTie2 (2 mg/kg) or PBS as control. The femurs were fixed in fresh 4% PFA at 4℃ overnight and then decalcified in 0.5 M EDTA solution (Sigma-Aldrich) for 14 days by exchanging the solution every 2 days. After decalcification, the femurs were paraffin-embedded and serial sections were prepared for immunohistochemistry. The sections were deparaffinized, dehydrated, and blocked with 3% H_2O_2 in methanol for 30 minutes at room temperature prior to staining. An endomucin antibody (Abcam ab106100) was incubated at 4℃ overnight and a biotinylated anti-rat IgG antibody (Dako) at room temperature for 30 minutes. TSA Biotin System Kit (PerkinElmer) and DAB (Vector Laboratories, Inc.) were applied to visualize the staining and the sections were counterstained with Fast Green (Sigma-Aldrich).

For histological evaluations of hearts after MI in ApoE−/− mice on HFD with siMCP1 (2 mg/kg) or siLuc treatment before and after surgery, mice were euthanized and hearts were perfused thoroughly with PBS and harvested. The hearts were embedded in O.C.T. compound (Sakura Finetek) and subsequently snap-frozen in a 2-methylbutane bath cooled with dry ice. For the scar area assessment, Masson's trichrome staining was performed according to manufacturer's instruction (Sigma-Aldrich). For each individual mouse, three evenly spaced short axis sections of the left ventricle were collected that sampled the infarct from basal to apical regions. The infarct size was calculated as (scar area slide 1 + scar area slide 2 + scar area slide 3) / (remote area slide 1 + remote area slide 2 + remote area slide 3) * 100%. For immunohistochemistry, 6 μm frozen sections were stained using antibodies: CD11b (BD Biosciences, clone M1/70), alpha-smooth muscle actin (αSMA, Abcam ab5694) and collagen I (Abcam ab21286). The appropriate biotinylated secondary

antibodies followed by VECTASTAIN ABC kit (Vector Laboratories, Inc.) were applied and AEC substrate (Dako) was used for color development. The sections were counterstained with Harris hematoxylin (Sigma-Aldrich). All the slides were scanned by using a digital scanner, NanoZoomer 2.0RS (Hamamatsu, Japan) and quantification was done using ImageJ. Three high-power fields per section per animal were analyzed.

ELISA

ELISAs for SDF1 and MCP1 (both R&D) in the bone marrow were performed by spinning (11.000 g, 2 min, 4°C) the bone marrow out of one femur and taking the supernatant for ELISAs, which were performed according to the manufacturers' instructions.

Statistics

The statistics were performed as published before[29]. Data are expressed as mean±SEM. Statistical analyses were performed using Prism (Version 7, GraphPad Software Inc). Two-sided student t test was used when two groups were compared and pretest for normality (D'Agostino-Pearson normality test; significance level 0.05) was not rejected. For nonparametric data Mann-Whitney test was used. If more then two groups were compared two-sided ANOVA tests followed by Bonferroni post-tests were applied. P values smaller than 0.05 indicate statistical significance.

Supplementary Material

Refer to Web version on PubMed Central for supplementary material.

Acknowledgements

References

1. Morrison SJ & Scadden DT The bone marrow niche for haematopoietic stem cells. Nature 505, 327–334 (2014). [PubMed: 24429631]

2. Mendelson A & Frenette PS Hematopoietic stem cell niche maintenance during homeostasis and regeneration. Nat Med 20, 833–846 (2014). [PubMed: 25100529]

3. Crane GM, Jeffery E & Morrison SJ Adult haematopoietic stem cell niches. Nature Reviews Immunology 17, 573–590 (2017).

4. Kaplan RN, Psaila B & Lyden D Niche-to-niche migration of bone-marrow-derived cells. Trends in Molecular Medicine 13, 72–81 (2007). [PubMed: 17197241]

5. Sipkins DA et al. In vivo imaging of specialized bone marrow endothelial microdomains for tumour engraftment. Nature 435, 969–973 (2005). [PubMed: 15959517]

6. Butler JM et al. Endothelial cells are essential for the self-renewal and repopulation of Notch-dependent hematopoietic stem cells. Cell Stem Cell 6, 251–264 (2010). [PubMed: 20207228]

7. Katayama Y et al. Signals from the Sympathetic Nervous System Regulate Hematopoietic Stem Cell Egress from Bone Marrow. Cell 124, 407–421 (2006). [PubMed: 16439213]

8. Gratwohl A et al. Hematopoietic stem cell transplantation: a global perspective. JAMA 303, 1617–1624 (2010). [PubMed: 20424252]

9. Giralt S et al. Optimizing autologous stem cell mobilization strategies to improve patient outcomes: consensus guidelines and recommendations. Biol Blood Marrow Transplant 20, 295–308 (2014). [PubMed: 24141007]

10. Swirski FK & Nahrendorf M Leukocyte behavior in atherosclerosis, myocardial infarction, and heart failure. Science 339, 161–166 (2013). [PubMed: 23307733]

11. Calado RT & Young NS Telomere maintenance and human bone marrow failure. Blood 111, 4446–4455 (2008). [PubMed: 18239083]

12. Seo A et al. Bone marrow failure unresponsive to bone marrow transplant is caused by mutations in THPO. Blood 130, 875–880 (2017). [PubMed: 28559357]

13. Whitehead KA, Langer R & Anderson DG Knocking down barriers: advances in siRNA delivery. Nature Reviews Drug Discovery 8, 129–138 (2009). [PubMed: 19180106]

14. Titze-de-Almeida R, David C & Titze-de-Almeida SS The Race of 10 Synthetic RNAi-Based Drugs to the Pharmaceutical Market. Pharmaceutical research 34, 1339–1363 (2017). [PubMed: 28389707]

15. Anselmo AC & Mitragotri S Nanoparticles in the Clinic. Bioeng Transl Med 1, 10–29 (2016). [PubMed: 29313004]

16. Yin H et al. Non-viral vectors for gene-based therapy. Nature reviews. Genetics 15, 541–555 (2014).

17. Kanasty R, Dorkin JR, Vegas A & Anderson D Delivery materials for siRNA therapeutics. Nature Materials 12, 967–977 (2013). [PubMed: 24150415]

18. Leuschner F et al. Therapeutic siRNA silencing in inflammatory monocytes in mice. Nature Biotechnology 29, 1005–1010 (2011).

19. Dahlman JE et al. In vivo endothelial siRNA delivery using polymeric nanoparticles with low molecular weight. Nature Nanotechnology 9, 648–655 (2014).

20. Dong Y et al. Lipopeptide nanoparticles for potent and selective siRNA delivery in rodents and nonhuman primates. Proc Natl Acad Sci USA 111, 3955–3960 (2014). [PubMed: 24516150]

21. Love KT et al. Lipid-like materials for low-dose, in vivo gene silencing. Proc Natl Acad Sci USA 107, 1864–1869 (2010). [PubMed: 20080679]

22. Khan OF et al. Ionizable Amphiphilic Dendrimer-Based Nanomaterials with Alkyl-Chain-Substituted Amines for Tunable siRNA Delivery to the Liver Endothelium In Vivo. Angewandte Chemie (International ed. in English) 53, 14397–14401 (2014). [PubMed: 25354018]

23. Khan OF et al. Dendrimer-Inspired Nanomaterials for the in Vivo Delivery of siRNA to Lung Vasculature. Nano Letters 15, 3008–3016 (2015). [PubMed: 25789998]

24. Whitehead KA et al. Degradable lipid nanoparticles with predictable in vivo siRNA delivery activity. Nature communications 5, 4277 (2014).

25. Khan OF et al. Endothelial siRNA delivery in nonhuman primates using ionizable low-molecular weight polymeric nanoparticles. Sci Adv 4, eaar8409 (2018). [PubMed: 29963629]

26. Chen D et al. Rapid discovery of potent siRNA-containing lipid nanoparticles enabled by controlled microfluidic formulation. Journal of the American Chemical Society 134, 6948–6951 (2012). [PubMed: 22475086]

27. Gref R et al. Stealth corona-core nanoparticles surface modified by polyethylene glycol (PEG): influences of the corona (PEG chain length and surface density) and of the core composition on phagocytic uptake and plasma protein adsorption. Colloids and surfaces. B, Biointerfaces 18, 301–313 (2000). [PubMed: 10915952]

28. Owens III DE & Peppas NA Opsonization, biodistribution, and pharmacokinetics of polymeric nanoparticles. International journal of pharmaceutics 307, 93–102 (2006). [PubMed: 16303268]

29. Heidt T et al. Chronic variable stress activates hematopoietic stem cells. Nat Med 20, 754–758 (2014). [PubMed: 24952646]

30. Xu C et al. Stem cell factor is selectively secreted by arterial endothelial cells in bone marrow. Nat Commun 9, 2449 (2018). [PubMed: 29934585]

31. Cheng M & Qin G Progenitor cell mobilization and recruitment: SDF-1, CXCR4, α4-integrin, and c-kit. Progress in molecular biology and translational science 111, 243–264 (2012). [PubMed: 22917234]

32. Furze RC & Rankin SM The role of the bone marrow in neutrophil clearance under homeostatic conditions in the mouse. The FASEB Journal 22, 3111–3119 (2008). [PubMed: 18509199]

33. Whitehead KA, Dahlman JE, Langer RS & Anderson DG Silencing or Stimulation? siRNA Delivery and the Immune System. Annual Review of Chemical and Biomolecular Engineering 2, 77–96 (2011).

34. Serbina NV & Pamer EG Monocyte emigration from bone marrow during bacterial infection requires signals mediated by chemokine receptor CCR2. Nat Immunol 7, 311–317 (2006). [PubMed: 16462739]

35. Nahrendorf M, Pittet MJ & Swirski FK Monocytes: protagonists of infarct inflammation and repair after myocardial infarction. Circulation 121, 2437–2445 (2010). [PubMed: 20530020]

36. Swirski FK et al. Ly-6Chi monocytes dominate hypercholesterolemia-associated monocytosis and give rise to macrophages in atheromata. J Clin Invest 117, 195–205 (2007). [PubMed: 17200719]

37. Tacke F et al. Monocyte subsets differentially employ CCR2, CCR5, and CX3CR1 to accumulate within atherosclerotic plaques. J Clin Invest 117, 185–194 (2007). [PubMed: 17200718]

38. Yvan-Charvet L et al. ATP-binding cassette transporters and HDL suppress hematopoietic stem cell proliferation. Science 328, 1689–1693 (2010). [PubMed: 20488992]

39. Nahrendorf M et al. The healing myocardium sequentially mobilizes two monocyte subsets with divergent and complementary functions. Journal of Experimental Medicine 204, 3037–3047 (2007). [PubMed: 18025128]

40. Panizzi P et al. Impaired infarct healing in atherosclerotic mice with Ly-6C(hi) monocytosis. J Am Coll Cardiol 55, 1629–1638 (2010). [PubMed: 20378083]

41. Itkin T et al. Distinct bone marrow blood vessels differentially regulate haematopoiesis. Nature 532, 323–328 (2016). [PubMed: 27074509]

42. Broxmeyer HE et al. Rapid mobilization of murine and human hematopoietic stem and progenitor cells with AMD3100, a CXCR4 antagonist. The Journal of Experimental Medicine 201, 1307–1318 (2005). [PubMed: 15837815]

43. Ferraro F et al. Diabetes impairs hematopoietic stem cell mobilization by altering niche function. Sci Transl Med 3, 104ra101 (2011).

44. Langen UH et al. Cell-matrix signals specify bone endothelial cells during developmental osteogenesis. Nat Cell Biol 19, 189–201 (2017). [PubMed: 28218908]

45. Peranteau WH, Hayashi S, Hsieh M, Shaaban AF & Flake AW High-level allogeneic chimerism achieved by prenatal tolerance induction and postnatal nonmyeloablative bone marrow transplantation. Blood 100, 2225–2234 (2002). [PubMed: 12200389]

46. Kwarteng EO & Heinonen KM Competitive Transplants to Evaluate Hematopoietic Stem Cell Fitness. J Vis Exp (2016).

47. Maryanovich M et al. The ATM-BID pathway regulates quiescence and survival of haematopoietic stem cells. Nat Cell Biol 14, 535–541 (2012). [PubMed: 22446738]
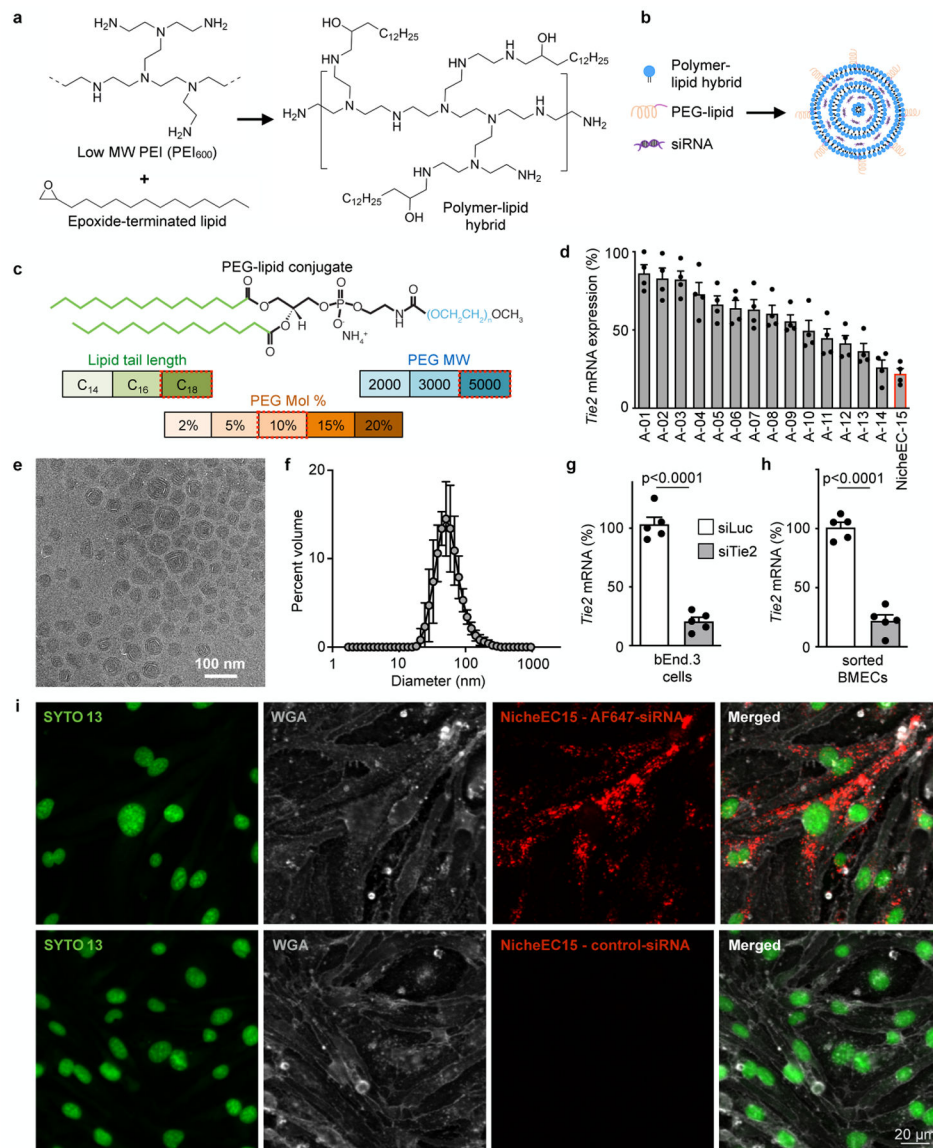
Figure 1 |. Composing a bone marrow endothelial cell (BMEC)-targeting nanoparticle.
a, Synthesis scheme of the epoxide-modified polymer-lipid hybrid material. **b**, Nanoparticles consisting of lipid hybrid, siRNA and a PEG-lipid conjugate were synthesized via microfluidic mixing. **c**, PEG-lipid conjugate parameters varied to form a library of unique nanoparticles for siRNA delivery to BMEC. Values outlined by red boxes indicate best silencing efficiency. **d**, Tie2 silencing in femoral bone marrow of C57BL/6 mice 48 h after injection of each nanoparticle containing siRNA against Tie2 (dosage: 1.0 mg/kg; n=4 mice per group; data are normalized to mRNA expression in naive mice). Strongest silencing was seen for NicheEC-15 highlighted in red. **e**, Cryo-TEM micrograph of NicheEC-15. **f**, Hydrodynamic diameter of NicheEC-15. **g**, **h** Tie2 silencing in bEnd.3 (**g**) and sorted BMEC (**h**) 24 hrs after addition of siLuc or siTie2 to the culture medium. Tie2 mRNA expression after exposure to siLuc was normalized to 100% (n=3 independent experiments (**g**) or 3 mice (**h**) per group; two-sided t-test). **i**, Confocal microscopy of bEND.3 cells 2 hrs after adding

NicheEC15 to the culture medium. Nuclei were stained with SYTO 13 and cell membranes with Wheat Germ Agglutinin (WGA). In the upper panels the nanoparticle was visualized by siRNA labeled with Alexa Fluor 647 (AF647); in the lower row an unlabeled control siRNA was used. This experiment was repeated twice with similar results. Data are shown as mean ± s.e.m.
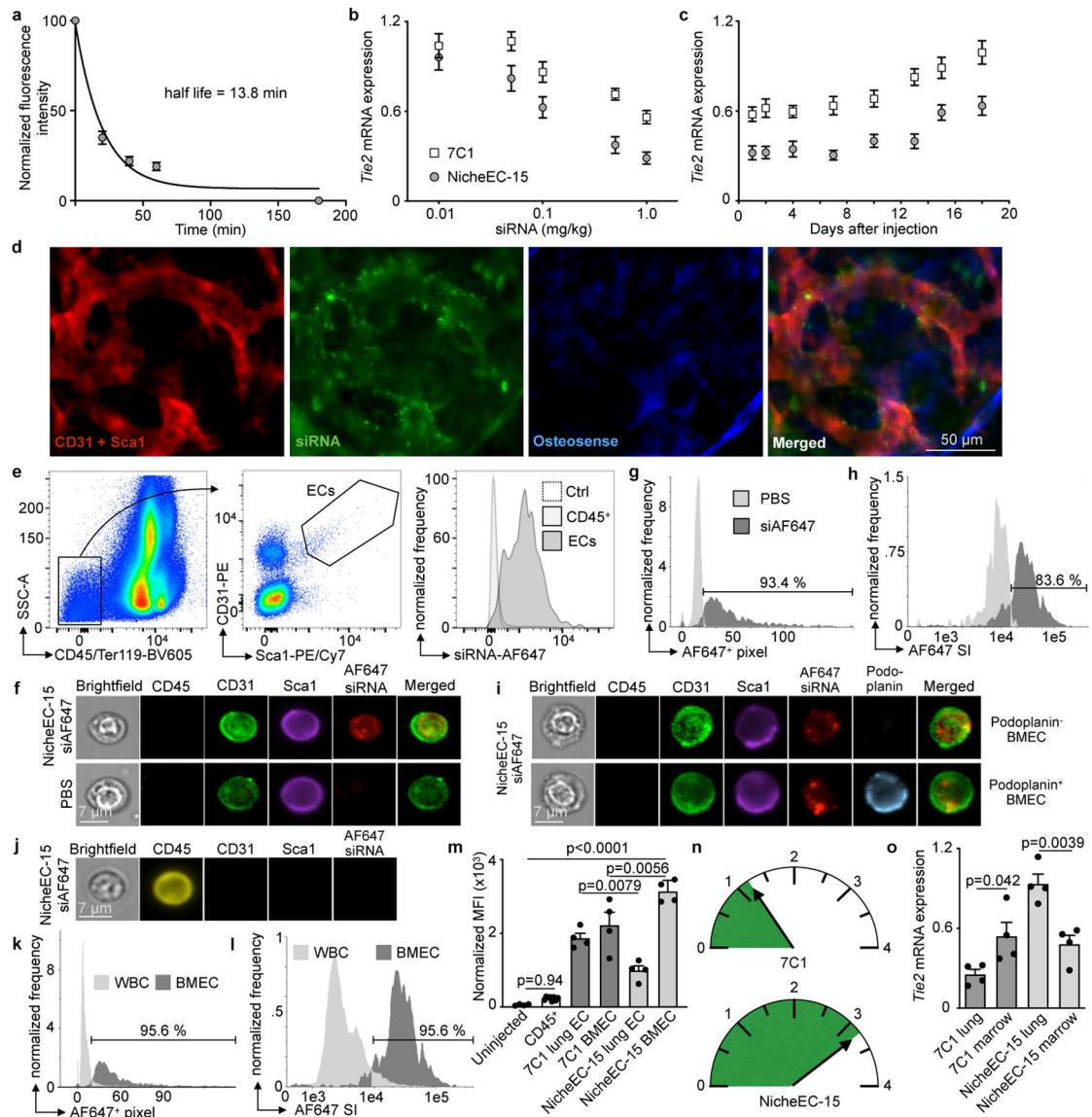
Figure 2 |. In vivo uptake of NicheEC-15 in BMEC.

a, Decline in blood fluorescence intensity was measured over time following a single injection of NicheEC-15 AF647-siRNA. The in vivo circulation half-life of NicheEC-15 was calculated to be 13.8 min (n=5 mice). **b**, Dose response curve of Tie2 silencing in whole bone marrow after in vivo injection of NicheEC-15 or 7C1 nanoparticles encapsulating siTie2 by bDNA assay (dose range 0.01 – 1.0 mg/kg, n=4 mice per group and time point). **c**, Time course of Tie2 expression in whole bone marrow following a single 1.0 mg/kg injection of NicheEC-15 or 7C1 encapsulating siTie2 by bDNA assay. Femurs were harvested 1–18 days post-injection (n=4 mice per group and time point). b, c, show fold changes in mRNA expression compared to naive mice. **d**, Intravital microscopy of the skull bone marrow 2 h after injection of NicheEC-15 with AF647-siRNA cargo. The vasculature was stained with PE labeled CD31 and Sca1 antibodies and Osteosense was used to visualize bone. **e**, Mice were sacrificed 2 h after IV injection of 2 mg/kg NicheEC-15

AF647-siRNA. BMEC were gated as shown in the FACS plots (left and middle panel). Histogram of endothelial cells (ECs) is shown with CD45+ leukocytes and ECs of uninjected control mice (right panel). **f**, ImageStream of endothelial cells 2 hrs after injection of NicheEC-15 AF647-siRNA compared to PBS injected controls (bottom). **g,h**, Uptake of the nanoparticle in endothelial cells compared to control mice injected with PBS. Of 816 endothelial cells 764 (93.4%) were positive for siAF647 based on (**g**) mean AF647 positive pixel number (=AF647$^+$ pixel) and 682 (83.6 %) on (**h**) peak cellular signal intensity for AF647 (=AF647 SI). **i**, ImageStream of endothelial cells 2 hrs after injection of NicheEC-15 AF647-siRNA with additional staining for podoplanin, identifying sinusoidal endothelial cells. **j**, ImageStream of leukocytes 2 hrs after injection of NicheEC-15 AF647-siRNA. **k,l**, Uptake of the nanoparticle in endothelial cells compared to leukocytes based on **k**, mean AF647 positive pixel number and **l**, peak cellular signal intensity for AF647. WBC indicates CD45+ leukocytes. Experiments **d-l** were repeated twice with similar results. **m**, Mean fluorescence intensity by flow cytometry of uninjected mice, CD45$^+$ leukocytes, BMEC and lung EC 2 hrs after injection of 2 mg/kg AF647-siRNA encapsulated into the 7C1 or NicheEC-15 nanoparticles (n=4 mice each, except CD45$^+$ n=8; one-way ANOVA with multiple comparisons). **n**, The mean fluorescence intensity (MFI) of BMEC was divided by MFI of lung EC for 7C1 and the NicheEC-15. The value is 1.19 for 7C1 and 3.17 for NicheEC-15. **o**, Comparison of Tie2 silencing in whole bone marrow and lung after in vivo injection of NicheEC-15 or 7C1 encapsulating siTie2 by a bDNA assay (dose: 1.0 mg/kg, n=4 mice each; two-sided t-test without multiple comparisons; fold changes in mRNA expression compared to naive mice). Data are shown as mean ± s.e.m.
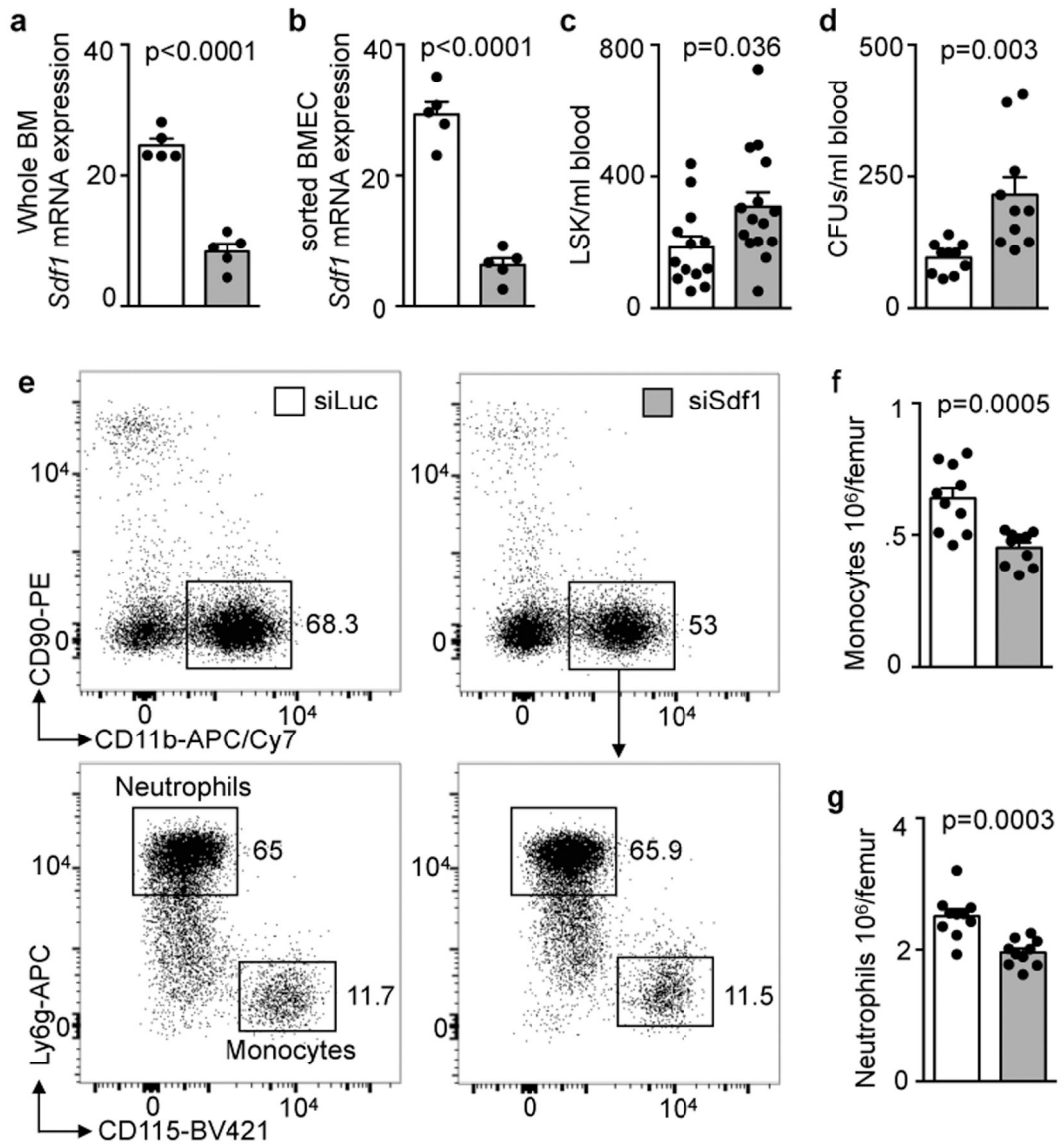
Figure 3 |. Effects of siSdf1 silencing on the bone marrow.
a, Sdf1 expression in whole bone marrow by qPCR (n=5 mice each). Mice were injected with 2 mg/kg siSdf1 or control siRNA targeting luciferase (siLuc) on day 0 and day 3 and harvested on day 5. **b**, qPCR for Sdf1 in sorted BMEC (n=5 mice each). **a**, **b**, were normalized to GAPDH expression. **c**, Number of blood LSK by flow cytometry. **d**, Colony forming units (CFUs) per ml of whole blood (n=10 mice each). **e**, Dot plots of bone marrow neutrophils and monocytes. Gating was performed in the sequence indicated by the arrow and highlighted gates from top to bottom. Numbers indicate the percentage of cells of the parent gate. Experiment was repeated twice with similar results. **f**, Number of monocytes and **g**, neutrophils per femur (n=10 mice per group). **a-d**, **f**, **g**, were analyzed using two-sided t-test. Data are shown as mean ± s.e.m.
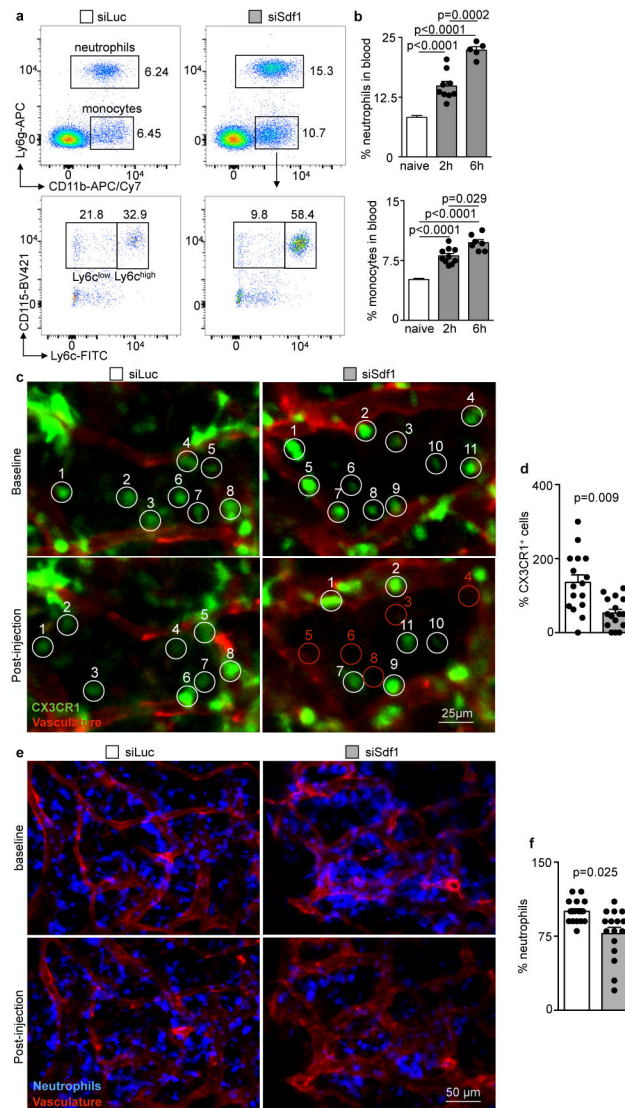
Figure 4 |. Release of bone marrow monocytes and neutrophils after siSdf1 treatment.
a, Representative dot plots 2 h after injection. Numbers shown indicate the percentage of cells of the parent gate. The experiment was repeated two times with similar results. **b**, Percentage of neutrophils (top panel) and monocytes (bottom panel) in the blood by flow cytometry (n=10 mice for naive and 2h, n=5 mice for 6h neutrophils and n=7 mice for 6h monocytes; two-way ANOVA with multiple comparisons). **c**, Intravital microscopy imaging of Cx3cr1^{+} cells in the skull bone marrow. Baseline images were taken before injection and cells were tracked by imaging every 10 to 30 min for a total of 2.5 hrs. The location of cells compared to baseline and at the last imaging after 2.5 hrs is highlighted with white circles. Red circles mark the area of cells that have left the niche. **d**, Percentage of Cx3cr1^{+} cells in the same area after 2.5 hrs compared to baseline which was adjusted to 100% (n=4 mice each, 4 fields of view per mouse; two-sided t-test). **e**, Same setup as in (c); neutrophils were labeled with Ly6g antibody. **f**, Similar to (d), the percentage of neutrophils after 2.5 hrs

compared to baseline (n=4 mice each, 4 fields of view per mouse; two-sided t-test). Data are shown as mean ± s.e.m.
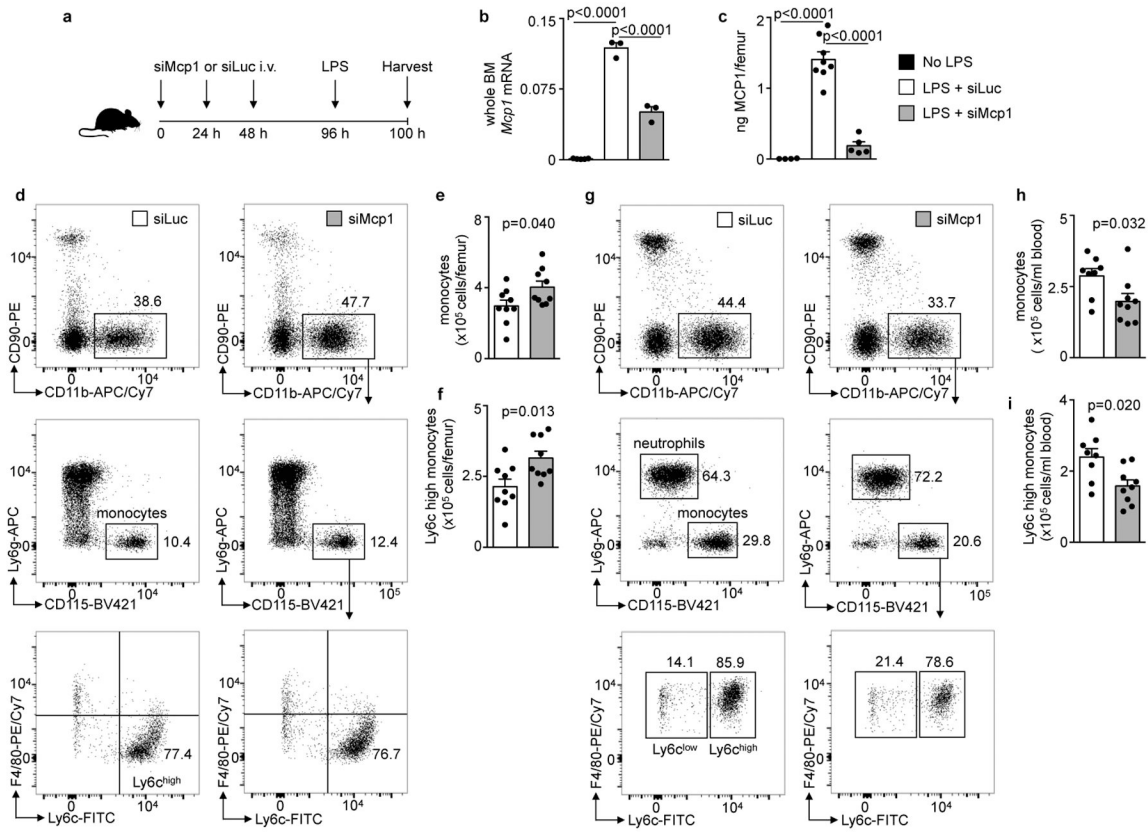
Figure 5 |. Effects of siMcp1 treatment during LPS-induced inflammation.
a, Experimental setup. **b**, Mcp1 expression in whole bone marrow by qPCR normalized to GAPDH expression (n=3 mice per group, except No LPS n=5; two-way ANOVA with multiple comparisons). **c**, Mcp1 levels by ELISA in bone marrow plasma (n=4, 7, and 5 mice per group, respectively; two-way ANOVA with multiple comparisons). **d**, FACS plots of bone marrow neutrophils and monocytes. Numbers shown indicate the percentage of cells of the parent gate. Gating was performed from top to bottom as indicated by the arrows. The experiment was repeated two times with similar results. **e**, Number of monocytes per femur. **f**, Number of Ly6c^{high} monocytes per femur. **g**, FACS plots of blood neutrophils and monocytes. Numbers indicate the percentage of cells of the parent gate. Gating was performed from top to bottom as indicated by the arrows. The experiment was repeated two times with similar results. **h**, Number of monocytes per ml of blood. **i**, Number of Ly6c^{high} monocytes per ml of blood. **e**, **f**, **h**, **i**, n=9 mice per group each; two-sided t-test. Data are shown as mean ± s.e.m.
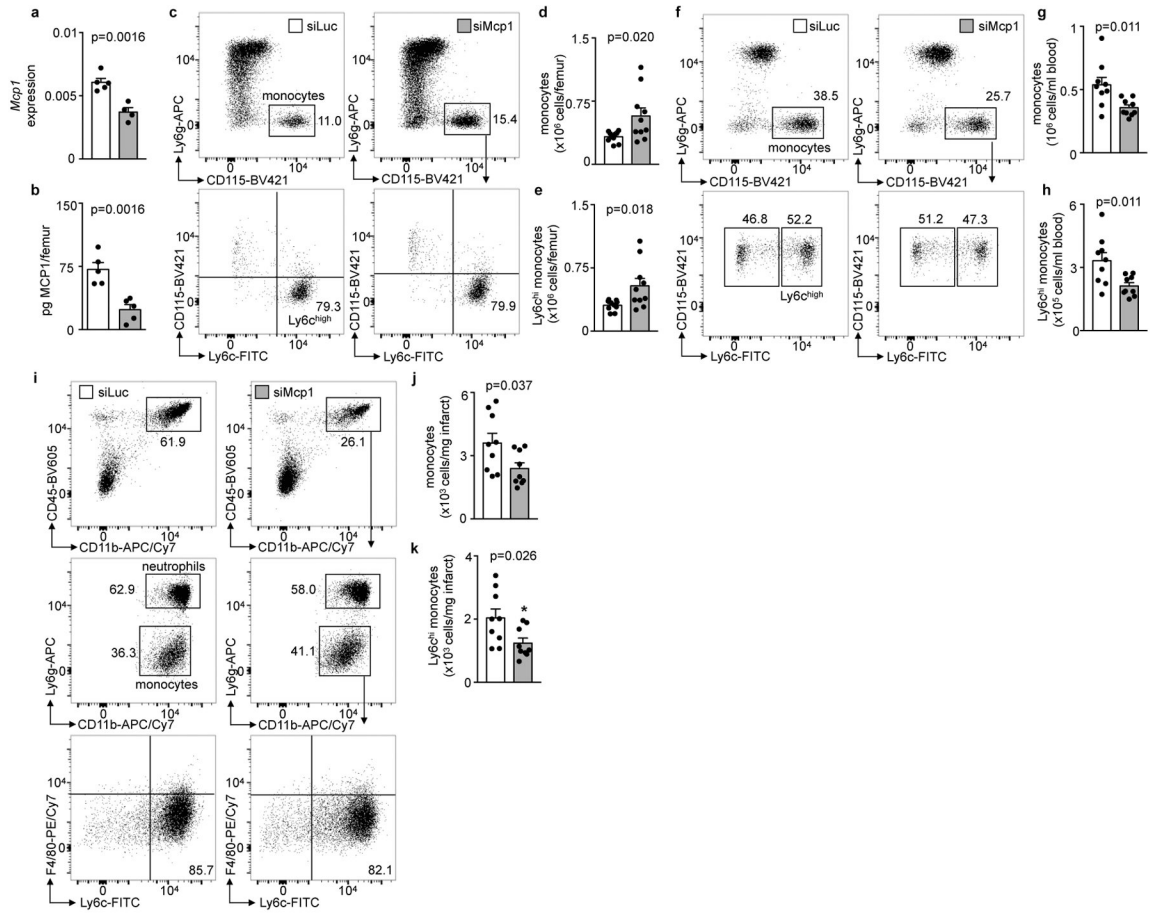
Figure 6 |. Effects of siMcp1 treatment on inflammatory cells 24 hrs after MI.

a, *Mcp1* expression in whole bone marrow by qPCR normalized to GAPDH expression. **b**, Mcp1 levels by ELISA in bone marrow plasma. **c**, FACS plots of bone marrow monocytes. Numbers shown indicate the percentage of cells of the parent gate. Gating was performed from top to bottom as indicated by the arrows. **a**, **b**, n=5 mice per group each; two-sided t-test. **d**, Number of monocytes per femur. **e**, Number of Ly6c^{high} monocytes per femur. **d**, **e**, n=10 mice per group each; two-sided t-test. **f**, FACS plots of blood neutrophils and monocytes. Numbers shown indicate the percentage of cells of the parent gate. Gating was performed from top to bottom as indicated by the arrows. **g**, Number of monocytes per ml of blood. **h**, Number of Ly6c^{high} monocytes per ml of blood. **i**, FACS plots of the infarct. Numbers shown indicate the percentage of cells of the parent gate. Gating was performed from top to bottom as indicated by the arrows. **j**, Number of monocytes per mg infarct tissue. **k**, Number of Ly6c^{high} monocytes per mg infarct tissue. **g**, **h**, **j**, **k**, n=9 mice per group each; two-sided t-test. Data are shown as mean ± s.e.m.
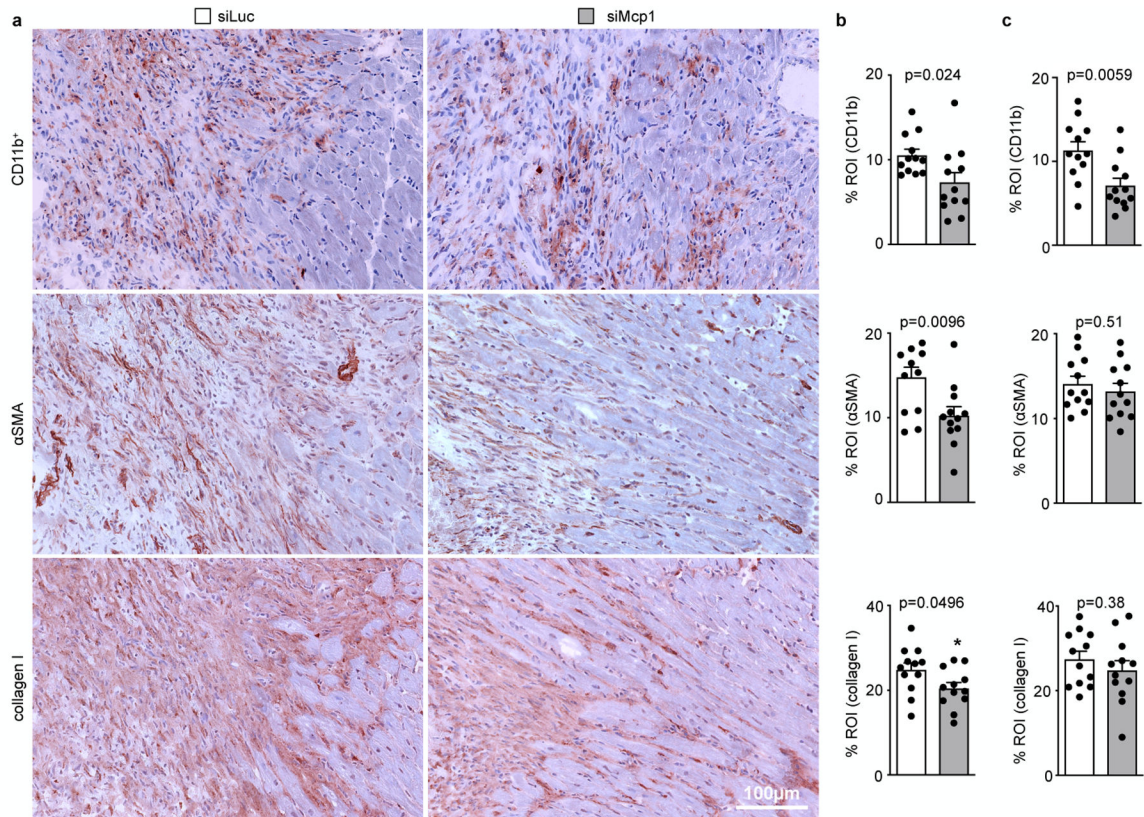
Figure 7 |. Cardiac effects of siMcp1 treatment 7 days after MI.
a, Immunohistochemical staining for myeloid cells (CD11b), α-smooth muscle actin+ fibroblasts (αSMA) and collagen deposition (collagen I) in the border zone of the infarct. After 10 weeks of HFD starting at 8 weeks of age MI was induced by permanent ligation of the LAD in ApoE$^{-/-}$ mice. Mice were either treated with siMCP1 or siLuc. **b**, Bar graphs show percentage of positive staining per region of interest (ROI) in the border zone of the infarct. **c**, Same analyses in the central infarct core. **a-c**, n=4 mice per group each and 3 fields of view per mouse; two-sided t-test. Data are shown as mean ± s.e.m.
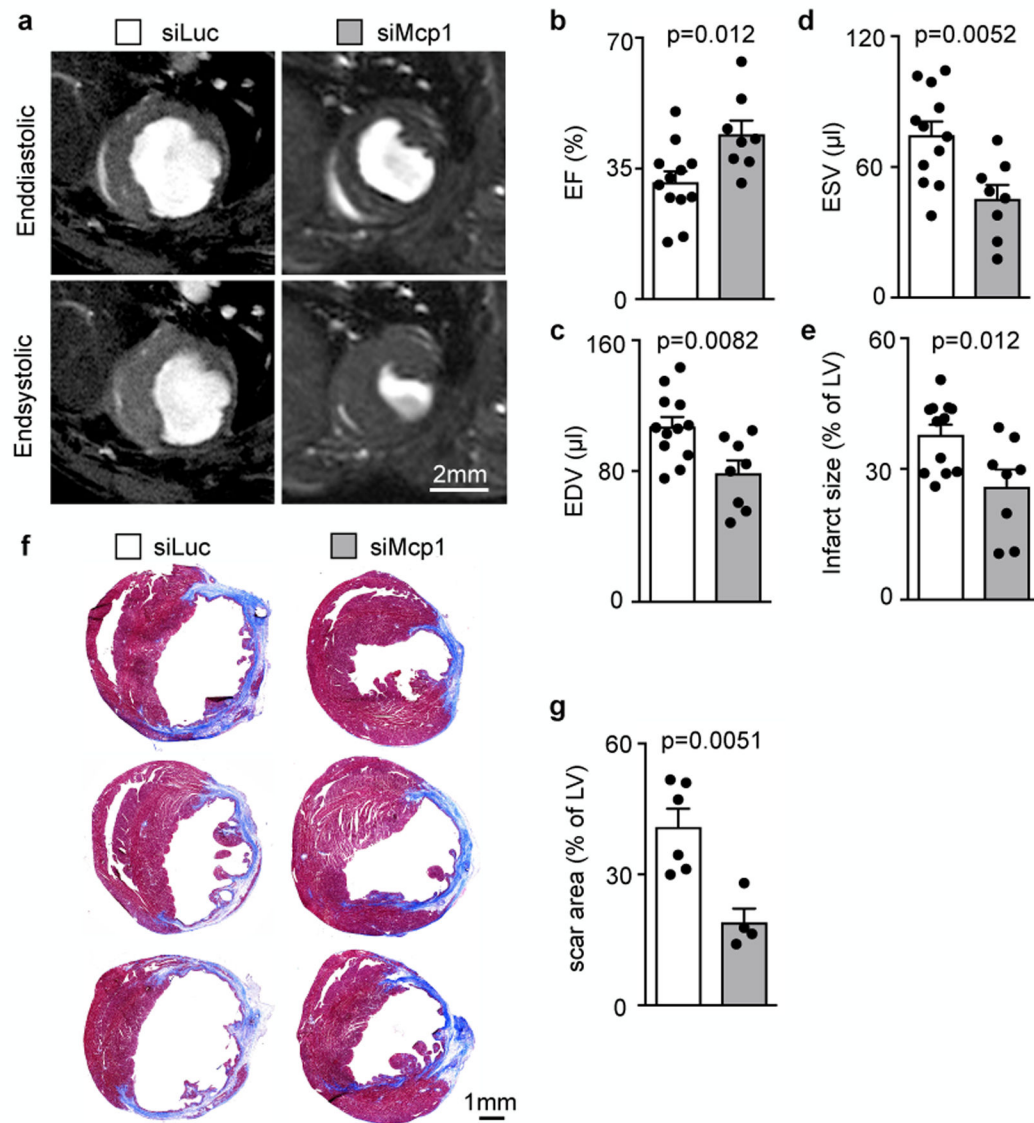
Figure 8 |. Therapeutic effects of siMcp1 on cardiac function and anatomy 3 weeks after MI.
a, Short axis magnetic resonance images 3 weeks after infarction. ApoE$^{-/-}$ mice were kept on high fat diet for 10 weeks starting at an age of 8 weeks before induction of MI by permanent ligation of the left coronary artery. Mice were treated with siMCP1 or control siLUC. **b**, Left ventricular ejection fraction (EF). **c**, Left ventricular end-diastolic volume (EDV). **d**, End-systolic volume (ESV). **e**, Fraction of the infarcted left ventricular wall volume by MRI. **a-e**, n=12 vs. 8 mice per group; two-sided t-test. **f**, Masson's trichrome staining is shown for n=3 mice per group. **g**, The scar was calculated as percent of left ventricular myocardium in three short axis views obtained in individual mice (n=5 mice each; two-sided t-test). Data are shown as mean ± s.e.m.